

# Theory of Mn-doped I-II-V Semiconductors

J. K. Glasbrenner,<sup>1</sup> I. Žutić,<sup>2</sup> and I. I. Mazin<sup>3</sup>

<sup>1</sup> National Research Council/Code 6393, Naval Research Laboratory, Washington, DC 20375, USA  
<sup>2</sup> Department of Physics, University at Buffalo, State University of New York, NY 14260, USA and  
<sup>3</sup> Code 6393, Naval Research Laboratory, Washington, DC 20375, USA

(Dated: September 18, 2018)

A recently discovered magnetic semiconductor  $\text{Ba}_{1-x}\text{K}_x(\text{Zn}_{1-y}\text{Mn}_y)_2\text{As}_2$ , with its decoupled spin and charge doping, provides a unique opportunity to elucidate the microscopic origin of the magnetic interaction and ordering in dilute magnetic semiconductors (DMS). We show that (i) the conventional density functional theory accurately describes this material, and (ii) the magnetic interaction emerges from the competition of the short-range superexchange and the longer-range spin-spin interaction mediated by the itinerant As holes. The latter can be viewed as a high-doping extrapolation of with the Schrieffer-Wolff  $p-d$  interaction representing an effective Hund's rule coupling,  $J_H^{\text{eff}}$ . The key difference between the classical double exchange and the actual interaction in DMS is that an effective  $J_H^{\text{eff}}$ , as opposed to the standard Hund's coupling  $J_H$ , depends on the Mn  $d$ -band position with respect to the Fermi level, and thus allows tuning of the magnetic interactions. The physical picture revealed for this transparent system may also be applicable to more complicated DMS systems.

*Introduction*-The dilute magnetic semiconductors (DMS) are nonmagnetic semiconductors doped with magnetic elements and displaying various manifestations of magnetic ordering [1–5]. The carrier-mediated magnetism in DMS offers a versatile control of the exchange interaction by tuning the Curie temperature  $T_C$  through changes in the carrier density, for example by an applied electric field, photoexcitations, or even heating [5–8]. However, despite the four decades of intensive work on DMS, challenges remain and materials complexity often hinders theoretical understanding. The origin of magnetic ordering [1–3, 5] and paths to higher  $T_C$  remain strongly debated [3, 9, 10].

The Mn-doping of II-VI and III-V semiconductors is the usual method for synthesizing DMS. In the II-VI DMS  $\text{Mn}^{2+}$  is isovalent with the group II ions and provides only spin doping; the lack of carriers makes robust ferromagnetism elusive. In the III-V compounds introducing Mn leads to both spin and carrier doping, but a low-solubility limit for Mn complicates growth and can lead to nanoscale clustering of Mn ions. This dual role of Mn complicates theoretical understanding and creates difficulties in establishing the connection between host properties and figures of merit. For example, the  $T_C$  for (Ga,Mn)N is predicted to be  $T_C > 300$  K [11], but in experiment it is much lower,  $T_C \lesssim 10$  K [12]. Finally, both substitutional and interstitial Mn are thermodynamically stable and form during synthesis, which additionally complicates theoretical treatment.

The recent discovery of the I-II-V DMS compounds [13–15] provides a way to overcome these difficulties. In contrast to the II-VI and III-V compounds, in the I-II-V ones hole and spin doping are controlled separately by substitution with the group I and group II ions, respectively. In  $(\text{Ba}_{0.7}\text{K}_{0.3})(\text{Zn}_{0.85}\text{Mn}_{0.15})_2\text{As}_2$ , a  $T_C \sim 220$  K [16] is already higher than  $\sim 190$  K [3] attained in (Ga,Mn)As, the prototypical III-V DMS. Unlike (Ga,Mn)As, both  $p$ - and  $n$ -doped I-II-Vs can be fer-

romagnetic [15, 17], and a coercive field  $\sim 10^4$  Oe in  $(\text{Ba,K})(\text{Zn,Mn})_2\text{As}_2$  at 2 K [15] is two orders of magnitude larger than in (Ga,Mn)As. Apart from potential applications [5], the I-II-V DMS compounds are well suited for theoretical study, because (1) the  $\text{Mn}^{2+}$  is isovalent with Zn, (2) charge is doped into the Ba sublayer, spatially and electronically disconnected from the active  $(\text{Zn,Mn})_2\text{As}_2$  layers, and (3) interstitial locations for Mn ions are energetically precluded.

A key feature that a theory of I-II-V DMS materials must capture is the curious result that despite the high-temperature measurements indicating a high spin state with  $5 \mu_B/\text{Mn}$ , the low-temperature ferromagnetic magnetization measurement finds moments of  $\lesssim 2 \mu_B$ . The authors of Ref. [15] conjectured that this reduction may be due to the formation of nearest neighbor  $\text{Mn}_2$  singlets. We will show below that this is a plausible explanation, noting that a correct theory should explain why singlets form and estimate their concentration.

In this Letter, we present density functional theory (DFT) calculations of the energetics of Mn pairs substituted in the Zn lattice as a function of the pair distance and hole-doping with K. We extract exchange parameters from these calculations and find that ordering changes from antiferromagnetic (AFM) with no hole doping to ferromagnetic (FM) with hole doping, with the exception of nearest neighbor (nn) pairs, which remain AFM and are energetically preferred. We then show using thermodynamic arguments that singlet formation is responsible for the reduced magnetization in Ref. [15]. We also address the different terminologies used for the effective magnetic interaction between the Mn  $d$  and As  $p$  states, such as double exchange [18], the Zener  $p-d$  model [19], and the RKKY interaction [20–22]. In our view, these all describe the same indirect exchange interaction [23] and therefore the same basic physics.

*Calculations*-We employed two DFT implementations: a pseudopotential method (VASP [24, 25]) and a full po-

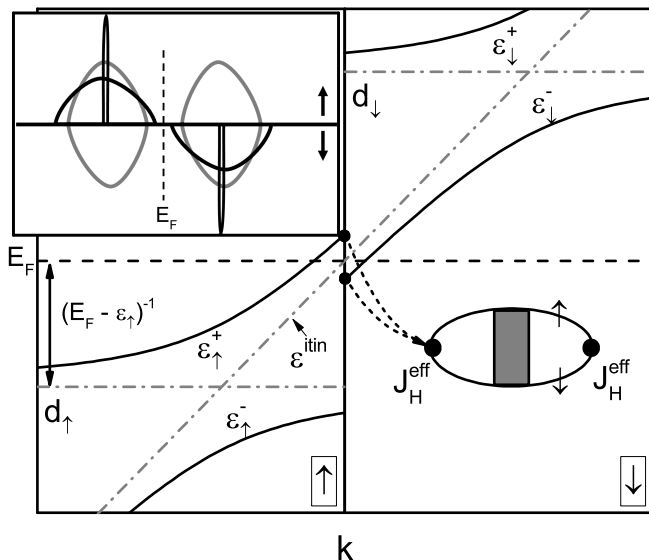


FIG. 1. A cartoon of the interaction between localized spins mediated by the itinerant carriers depicting a spin-resolved schematic of the broad As band  $\varepsilon^{\text{itin}}$  hybridizing with the narrow Mn bands  $d_{\uparrow}$  and  $d_{\downarrow}$ , forming the bands  $\varepsilon_{\uparrow,\downarrow}^{\pm}$ . The effective magnetic coupling  $J_H^{\text{eff}}$  scales with  $(E_F - \varepsilon_{\uparrow})^{-1}$ . Inset: A schematic of the  $\text{BaZn}_2\text{As}_2$  DOS before (gray lines) and after (black lines) Mn doping. The narrow Mn states interact with the As states, broadening the DOS and reducing the indirect band gap.

tential linear augmented plane wave (LAPW) method (ELK [26]). Selected results have been verified against an alternative LAPW package, WIEN2k [27]. A generalized gradient approximation [28] was used for total energy calculations and the modified Becke-Johnson functional [29, 30] (known to give correct band gaps for semiconductors) was used for analyzing the electronic structure. For pure  $\text{BaZn}_2\text{As}_2$  we obtain the indirect gap of 0.25 eV between the  $\Gamma$  and  $Z$  points, and the direct gap of 0.71 eV at the  $\Gamma$  point, in agreement with previous calculations [31], see Supplementary Material.

We first analyze the effect of Mn doping ( $\text{Ba}(\text{Zn}_{1-y}\text{Mn}_y)_2\text{As}_2$ ,  $y > 0$ ). The inset in Fig. 1 qualitatively illustrates the spin-resolved density of states (DOS) (see Supplementary Material for explicit DOS calculations). There are five Mn bands in each spin, confirming the  $\text{Mn}^{2+}$  state. The calculated Mn moment is  $\sim 4.7 \mu_B$  in ELK and  $\sim 4.9 \mu_B$  in VASP [32]. The valence band is predominantly As  $p$  states, the conduction band Ba states. The As states hybridize with Mn as depicted in Fig. 1, which is parameterized by hopping parameter  $t_{pd}$  [33]. As a result, the top of the As spin-majority band is pushed up and the bottom down at a rate of  $\sim 2.8y$  eV, so for  $y = 0.25$ , there is a shift of 0.7 eV. In contrast, the bottom of the conduction (Ba) spin-minority band is pushed down because of the hybridization with unoccupied Mn states.

This provides the magnetic coupling between the local spin and itinerant carriers [34]. Another manifestation of the same effect, verifiable experimentally, is that with Mn doping the indirect gap between the top of the spin-up valence band and the bottom of the spin-down conduction band is reduced and eventually closes when the doping is large enough, see the inset of Fig. 1.

By introducing hole doping [ $\text{Ba}_{1-x}\text{K}_x(\text{Zn}_{1-y}\text{Mn}_y)_2\text{As}_2$ ,  $x > 0$ ], the calculated Mn moments change. At  $x = 0.4$  they are reduced by 40% and As atoms acquire opposite moments (Ba and Zn remain unpolarized). Both effects are caused by the Mn-As hybridization, while K doping makes the effect visible. Indeed, because of the upshift of the top of the As band, there are more holes in the spin-majority band, creating negative polarization on As. Furthermore, because of proximity the hybridization of As holes with the spin-majority Mn states is stronger than with the spin-minority ones, so holes carry more spin-majority Mn character and hole-doping reduces the Mn moments.

Next we constructed different supercells, placing Mn pairs into different substitutional positions. Unlike (Ga,Mn)As, where Mn easily occupies interstitials, complicating the theoretical analysis, in  $\text{BaZn}_2\text{As}_2$  this is essentially impossible. The calculated free energy penalty for interstitial vs substitutional Mn doping is huge,  $F_{\text{int}} - F_{\text{sub}} > 2.4$  eV/Mn, for all admissible values of the Zn chemical potential (see Supplementary Material).

We now assume a Heisenberg model for the Mn-Mn magnetic interactions at lattice sites  $i, j$ ,

$$H = \sum_{i < j} J_x^{ij} \hat{S}_i \cdot \hat{S}_j, \quad (1)$$

where the  $\hat{S}_{i,j}$  are the unit vectors in the spin directions. We can map [35] the calculated energies for different magnetic configurations onto Eq. (1) and extract the spatial dependence of the exchange  $J_x^{ij}$ .

Figure 2(a) summarizes  $J_x^{ij}$  for both intraplanar and interplanar Mn pairs up to 7 neighbors for  $x = 0, 0.2$ , and 0.4 hole dopings (for more details, see the Supplementary Material). We note that the intraplanar and interplanar results roughly lie on the same universal curve, so we define  $J_x(r) \equiv J_x^{ij}$ . Without hole doping ( $x = 0$ ),  $J_x(r)$  is AFM for all pairs and decays strongly with distance, consistent with superexchange [18, 23].

Hole doping drives the system toward ferromagnetism, so that  $J_x(r)$  becomes FM for 2nd and higher neighbors. For nn pairs,  $J_x(r)$  remains AFM even for  $x = 0.4$ , but is reduced threefold. This reduction, along with the 2nd neighbor's exchange parameter barely changing sign to become FM for  $x = 0.2$ , reveals that this behavior is due to the competition between the short-range AFM superexchange and a longer-range FM interaction.

We now address the puzzling reduction of the net magnetization  $M$  compared with the local Mn magnetic moments. We verified that even for  $x = 0.4$  doping that the nn exchange parameter is AFM, such that nn Mn pairs form a singlet. Let us first assume that Mn dopants

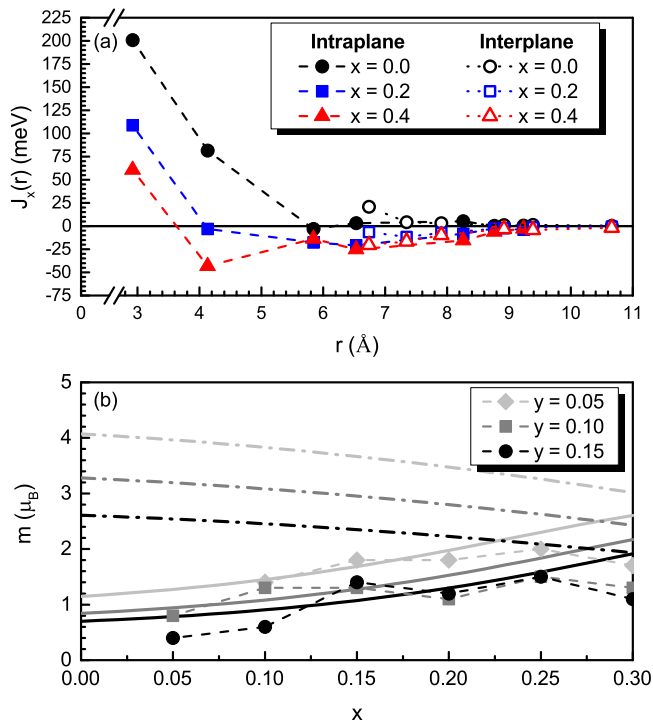


FIG. 2. (Color online) The magnetic interaction’s doping dependence. (a) The exchange coupling  $J_x(r)$  as a function of distance between Mn pairs for different hole dopings  $x$ . (b) The dependence of the reduced magnetization due to singlet formation on hole doping. The symbols are the experimental measurements from Ref. [15]. The solid lines are the reduced magnetization when Mn singlet formation is in thermodynamic equilibrium at 500 K, while the dash-dot lines are the reduced magnetization for a random distribution of Mn atoms. The light gray lines correspond to  $y = 0.05$ , the dark gray lines to  $y = 0.10$ , and the black lines to  $y = 0.15$ .

are randomly distributed in the Zn lattice and estimate the magnetization reduction. If we neglect clusters of 3 or more Mn atoms (i.e., assuming  $y \ll 1$ ), we obtain  $M_{\text{theor}}(x, y) = M(x)(1 - y)^4$ . Depending on  $x$ ,  $M(x) \approx 3\text{--}5 \mu_B$ , and we can interpolate  $M(x)$  using our results. Figure 2(b) shows  $M_{\text{theor}}(x, y)$  for three values of  $y$  (dash-dotted lines) and compares it with the experiment of Ref. [15]. While there is some qualitative agreement, the magnetization suppression is noticeably underestimated, especially for small  $x$ .

Our calculations also indicate an energetic preference for nn Mn pairs to form. This, along with the variation in experimental Mn moments, leads us to conclude that the suppression is sensitive to sample preparation and hence the Mn distribution is not entirely random. To quantify this, we use the calculated energy differences between the AFM nn pair and a remote FM pair:  $\Delta E(x) \sim 185, 80$  and  $-30$  meV, for  $x = 0, 0.2$  and  $0.4$ , respectively. We can now evaluate the free energy using these values and the combinatorial entropy (see the Supplementary Material) to obtain the moment reduction

$r = (\sqrt{\beta^2 + 16\beta y} - \beta)/8y$ , correct in the  $y \ll 1$  limit, where  $\beta = \exp[-\Delta E/T]$ . Interpolating the calculated  $\Delta E(x)$  and  $M(x)$ , and using as the effective synthesis temperature 500 K [36], we get the solid lines shown in Fig. 2(b). Given the variation in the experimental data and the lack of any adjustable parameter, the agreement is excellent. From these calculations we can predict that quenching, rather than slow cooling, may be advantageous for enhancing the magnetization per Mn, which can be as high as  $3 \mu_B$ .

*Discussion*—We determined that the magnetic ordering is a combination of a short-range AFM interaction and a longer-range FM interaction. We identify the AFM interaction as superexchange, which is compatible with Mn being in the high-spin  $S = 5/2$  state, and is accounted for in DFT. The basic picture of superexchange is that there is an effective amplitude  $t_{dd}$  for a  $d$ -electron to hop from one Mn to another. For nn pairs  $t$  is large, as only one intermediate hop to an As  $p$  state is required, and in addition there is some direct overlap between Mn  $d_{x^2-y^2}$  orbitals. If the alignment is FM, hopping leads to a splitting of the occupied Mn states with no gain in kinetic energy. For an AFM alignment, where hopping proceeds from occupied to unoccupied states, this leads to a downshift of the occupied Mn states by  $2t_{dd}^2/U$ , where  $U$  is the energy cost of flipping the spin of one  $d$  electron. This cost in DFT is  $\sim 5J_H$ , where  $J_H \sim 0.8$  eV is the Hund’s rule coupling in Mn (in the Hubbard model  $U$  comes from the Coulomb repulsion and may be larger than  $5J_H$ ). This creates the superexchange coupling  $J_{SE} \approx 2t_{dd}^2/U$ . For farther neighbors the hopping probability involves multiple hoppings via high-lying Zn states and rapidly decays.

We will argue now [37] that the long-range FM ordering is a version of double exchange (DE) [18], but first we give an overview of the DE interaction. The original model [19] assumed a strong Hund’s coupling between localized spins and itinerant electrons from the same atomic species, which in practice is due to non-integer valency, and has led to the misconception that DE itself *requires* mixed valency. Instead, the only real requirement is that the interaction of the local spins with itinerant electrons be described by an operator of the form  $J_H \hat{S} \cdot \hat{\sigma}$ . Note that the nature and sign of  $J_H$  does not matter, because in the end  $J_H$  is squared.

The other essential ingredient of DE was the itinerant carriers delocalizing to lower their kinetic energy, which preferred a FM arrangement of the local spins. In the original model [19] the strong coupling limit  $J_H \rightarrow \infty$  was assumed in order to simplify the calculations, but that was not a necessary condition for DE. The DE picture, that of itinerant electrons adjusting their spin density to the background of local spins with some configurations being more energetically preferable, is simply the standard spin response theory described in the weak coupling regime by the linear spin susceptibility  $\chi(q)$ . In general  $\chi(q)$  depends on the electronic structure and Fermi surface geometry, so again for simplicity it is often approxi-

mated by its value at the  $\Gamma$  point,  $\chi(q) = \chi(0) = N_{\uparrow}(0)$ , which is not a bad approximation when all sites contain a local moment. Again, we note that this approximation is not essential when defining DE. Finally, if the concentration of itinerant carriers is small such that the Fermi length  $2\pi/k_F \gg d$  ( $d$  is the average distance between spins), then the response is FM for all relevant distances. For larger  $d$  the response decays rapidly and might acquire an oscillatory part, which depends on the Fermi surface. This is known as the RKKY interaction [20–22].

To review, the general picture is that the DE implies a local spin interacting via exchange with an itinerant sea of carriers, which itself responds by adjusting its spin density to align with the other localized spins, and then another of these localized spins interacts via exchange with the sea. There are two elementary exchange processes involved, see the diagram in Fig. 1, hence DE. In other words, DE and RKKY are two different sides of the same coin.

With this clarified, we now turn to the details of the effective exchange interaction between the local Mn spins and itinerant As holes. As discussed, in DFT the As electrons at the Fermi level hybridize with Mn and acquire spin-splitting, see Fig. 1. The upshift of spin-majority states at the Fermi energy is  $5Zt_{pd}^2/(E_F - \varepsilon_{\uparrow})$  (the bottom of the As band shifts *down*), where  $Z = 4$  is the Mn-As coordination number. Here the spin-minority Mn states are located at  $\varepsilon_{\downarrow} > E_F$ , and the spin majority ones at  $\varepsilon_{\uparrow} < E_F$ , and, for simplicity, the hopping amplitude  $t_{pd}$  is assumed to be the same for all Mn  $d$  states. Similarly, the spin minority bands are shifted down by  $5Zt_{pd}^2/(\varepsilon_{\downarrow} - E_F)$ . This yields an effective Mn spin splitting and thus an effective Hund’s rule coupling of

$$J_H^{\text{eff}} = \frac{-Zt_{pd}^2(\varepsilon_{\uparrow} - \varepsilon_{\downarrow})}{(E_F - \varepsilon_{\uparrow})(\varepsilon_{\downarrow} - E_F)} = \frac{-Zt_{pd}^2U}{(E_F - \varepsilon_{\uparrow})(\varepsilon_{\uparrow} + U - E_F)}.$$

This is formally the same as the Schrieffer-Wolff transformation frequently used for Kondo systems [18, 34]. The DMS literature typically refers to this as the  $p-d$  model. We emphasize that the  $p-d$  model [23] is not an alternative to DE, but a modification of the latter, where  $J_H$  is replaced with  $J_H^{\text{eff}}$ . The RKKY theory is in the same spirit, modifying the same physics in a different way by lifting the  $q = 0$  approximation, in weak coupling, and using a  $q$ -dependent susceptibility. In all cases the effective coupling appears as a pair of vertices attached to a polarization bubble as in Fig. 1, and so the sign of  $J_H^{\text{eff}}$  is irrelevant.

Unlike  $J_H$ , in principle  $J_H^{\text{eff}}$  is tunable by changing the spin-flip energy cost  $U$  and the position of the occupied  $d$ -level  $\varepsilon_{\uparrow}$ . In our DFT calculations  $E_F - \varepsilon_{\uparrow} \sim U/2$ , which is the least advantageous situation. We suggest that substituting As with Sb or P may shift  $\varepsilon_{\uparrow}$  up or down, yielding a  $E_F - \varepsilon_{\uparrow}$  closer to  $U/5$  or  $4U/5$  and increasing  $J_H^{\text{eff}}$  by  $\sim 60\%$ . Assuming that other parameters remain unchanged, an enhancement of exchange coupling could increase  $T_C$  by a factor of 2.5, which suggests a path

forward to room-temperature FM ordering in the I-II-V compounds.

*Conclusions*—We have shown, based on our first principles calculations, that ferromagnetism in  $(\text{Ba,K})(\text{Zn,Mn})_2\text{As}_2$  is a result of the interaction of localized Mn spins with itinerant As holes that have a ferromagnetic spin response for all relevant Mn-Mn distances, except for nearest neighbors. This is a variant of the classical double exchange with the simple modification of replacing the Hund’s coupling  $J_H$  by the effective  $p-d$  coupling  $J_H^{\text{eff}}$ .

The nearest neighbor magnetic interaction is a combination of Anderson’s superexchange that is weakened, but not overcome, by the ferromagnetic double exchange, and for a K concentration less than  $\sim 0.35$  it is energetically advantageous for Mn to form nearest neighbor singlet pairs. Our calculations describe this process quantitatively and predict a net magnetization reduction from the ideal  $5 \mu_B/\text{Mn}$  in excellent agreement with experiment.

While our findings have focused on the  $(\text{Ba,K})(\text{Zn,Mn})_2\text{As}_2$  compound, we believe that the transparent and simple physical picture that has emerged from studying this unique system is more general and applicable to other DMS compounds. Our theory and calculations are uncomplicated by multiple chemical issues common to other generations of DMS compounds such as Mn-doped IV-VI, III-V, and II-VI materials. Thus, this new generation of I-II-V materials is an exciting playground for experimentalists and theorists alike and deserves further study to elucidate the intrinsic physics of DMS materials.

*Acknowledgments*—We are grateful to A. Petukhov, F. Ning, and C. Q. Jin for their useful discussions. I.I.M. acknowledges funding from the Office of Naval Research (ONR) through the Naval Research Laboratory’s Basic Research Program. J.K.G. acknowledges the support of the NRC program at NRL. I. Z. was supported by DOE-BES Grant No. de-sc0004890 and ONR.

## SUPPLEMENTARY MATERIAL

*Additional computational details*—A schematic of the crystal structure of  $\text{BaZn}_2\text{As}_2$  is depicted in Fig. 3(a).  $\text{BaZn}_2\text{As}_2$  belongs to space group  $I4/mmm$ , and for our calculations we used the experimental lattice constants  $a = 4.131 \text{ \AA}$  and  $c = 13.481 \text{ \AA}$ . These constants are taken from the experiment in Ref. [15] and correspond to the co-doped  $(\text{Ba,K})(\text{Zn,Mn})_2\text{As}_2$  system. The Wyckoff sites for the atoms are  $2a$ ,  $4d$ , and  $4e$  for Ba, Zn, and As respectively, and the internal parameter for As is set to  $z_{\text{As}} = 0.3645$ . For all supercells of  $\text{BaZn}_2\text{As}_2$  with Mn pairs substituted for Zn atoms, we relax the internal atomic positions in VASP for the ferromagnetic (FM) and antiferromagnetic (AFM) magnetic configurations. The  $a$  and  $c$  lattice parameters are not relaxed, as the doping in our system is light and in an experimental system

would have a negligible effect on these parameters.

The virtual crystal approximation (VCA) was used to simulate hole-doping (in experiment it is the substitution of K for Ba), and the implementation depends on the code used. The VCA in ELK is implemented in the standard way, by introducing a fictitious atom at the Ba sites which has a fractional charge between that of Cs and Ba, such as  $Z = 55.6$ . For VASP, the VCA corresponds to a weighted average of the pseudopotentials for Ba and K, such as 80% Ba and 20% K. The electronic structure generated using this method is consistent with the electronic structure obtained using the VCA in ELK. We note that atomic relaxation is not possible when using the VCA in VASP, so we take the relaxed structure from the Ba(Zn,Mn)<sub>2</sub>As<sub>2</sub> supercells. The use of the VCA in both ELK and VASP is reasonable as there are no Ba states near the Fermi energy and this approach has been used successfully on the similar compound BaMn<sub>2</sub>As<sub>2</sub> [38] as well as in isostructural Fe-based superconductors.

*Electronic structure*-The band structure of pure BaZn<sub>2</sub>As<sub>2</sub> calculated using ELK and the modified Becke-Johnson (mBJ) functional [29, 30] is in Fig. 4. The band character is indicated in the legend. The valence band maximum is primarily As states and the conduction band minimum is primarily Ba states with a small amount of Zn character. Finally, the LAPW electronic structure for pure BaZn<sub>2</sub>As<sub>2</sub> is in excellent agreement with that generated by the pseudopotential method also using the mBJ functional.

The density of states (DOS) for BaZn<sub>2</sub>As<sub>2</sub>, obtained using VASP and the mBJ functional, is shown in Fig. 5, where the total DOS and the Mn partial DOS are both shown. The partial DOS of Mn confirms that it is in the Mn<sup>2+</sup> state.

*Details of calculating  $J_x^{ij}$* -The Heisenberg Hamiltonian,

$$H = \sum_{i<j} J_x^{ij} \hat{S}_i \cdot \hat{S}_j, \quad (2)$$

defines the exchange parameter  $J_x^{ij}$  for Mn-Mn pairs placed in the Zn lattice. The Mn atoms are substituted in the two-dimensional Zn lattice as shown in Fig. 3(b), which for a Mn atom fixed at site 0 indicates which other site is the 1st nearest neighbor, 2nd nearest neighbor, etc. We constructed supercells of different dimensions and placed two Mn atoms in the Zn lattice at different sites. Let us define the  $1 \times 1 \times 1$  unit cell to be the conventional 10 atom cell with dimensions  $a \times a \times c$  with two Zn layers as depicted in Fig. 3(a). The dimensions of the supercells we used in our calculations are then summarized in Table I along with the Mn doping level  $y$  from substituting two of the Zn atoms with Mn atoms.

To extract the exchange parameter, we calculated the energy difference  $E_{AFM} - E_{FM}$  for an AFM and FM alignment of the Mn moments in VASP for the various supercells. These calculations were carried out for hole-doping concentrations of  $x = 0.0$ ,  $x = 0.2$ , and  $x = 0.4$  in the VCA. The intraplane and interplane neighbors used

in our calculations for each supercell dimension are summarized in Table I, which refer to the neighbor pairings indicated in Fig. 3(b). The energies for the intraplane FM and AFM alignments in the  $3 \times 3 \times 1$  supercell are reported in Table III for the different hole-doping levels. Finally, the magnitudes of the extracted exchange parameters and their standard errors for the different hole-doping levels are summarized in Table II. Note that the listed errors do not reflect inaccuracy of the DFT calculations, but rather the standard errors of the fitting procedure. Physically, it corresponds to the Heisenberg model not being an entirely accurate description of the exchange interaction in metallic systems.

*Mn-Mn pair distribution*-In the main text we discuss that the reduction of the measured moment of Mn in experiment can be understood using a thermodynamic argument. In short, a statistical calculation of the entropy of the chance of one Mn atom having another Mn for a neighbor in the thermodynamic limit yields an expression for the reduction of the total magnetization per Mn atom. Here, we explicitly derive this expression.

Let there be  $m$  Mn atoms that occupy sites on a two-dimensional square lattice with  $n$  sites. The total number of bonds in this system is  $2n$  and there are  $k$  Mn-Mn dimers. The total number of possible ways to populate these  $2n$  bonds with  $k$  dimers is

$$\binom{2n}{k} = \frac{(2n)!}{k!(2n-k)!}. \quad (3)$$

This leaves  $m - 2k$  Mn atoms to populate the remaining  $n - 2k$  sites, and the total number of ways to do this is

$$\binom{n-2k}{m-2k} = \frac{(n-2k)!}{(n-m)!(m-k)!}. \quad (4)$$

The total combinations for decorating the square lattice is the product of Eqs. (3) and (4), which we define as  $W$ . This is correct only in the dilute regime  $m \ll n$ , as we neglect instances where any of the remaining  $(n - 2k)$  Mn atoms ends up next to a dimer, as well as the possibility that two dimers border each other at a right angle.

We now approximate the factorials using Stirling's formula,

$$n! \approx \sqrt{2\pi n} (n/e)^n, \quad (5)$$

take the logarithm of  $W$  and expand in  $1/n$  (again, possible in the dilute limit). The resulting entropy is

$$S = \ln \left( \frac{2^{k-1} \left(\frac{k}{e}\right)^{-k} e^{m-k} e^{k-m} \left(\frac{m-2k}{e}\right)^{2k-m} n^{m-k}}{\pi \sqrt{k} \sqrt{m-2k}} \right). \quad (6)$$

We now substitute  $m = yn$ ,  $k = \kappa n$ , and write down the free energy  $F$  per site,

$$-\frac{F}{T} = -\kappa \frac{\Delta E}{T} + \frac{S}{n}, \quad (7)$$

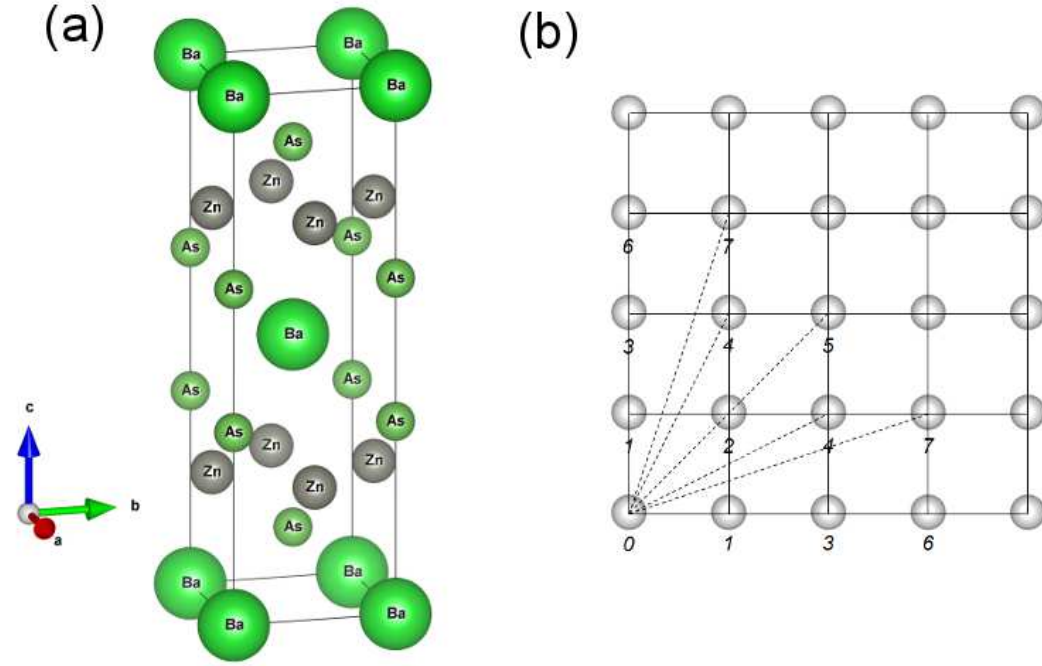


FIG. 3. (Color online) (a) The crystal structure of the tetragonal  $\text{ThCr}_2\text{Si}_2$  phase of  $\text{BaZn}_2\text{As}_2$ . (b) A schematic view of the two-dimensional Zn planes. The labels indicate the neighbor numbers with one Mn fixed at site 0 and another placed at sites 1-7. The nearest neighbor interaction connects sites 0 and 1, the 2nd nearest neighbor interaction connects sites 0 and 2, and so on. For the interplane interactions, the nearest interplane neighbor interaction connects site 0 in one plane with site 0 in the neighboring plane, the 2nd nearest interplane neighbor interaction connects site 0 in one plane with site 1 in the neighboring plane, and so on.

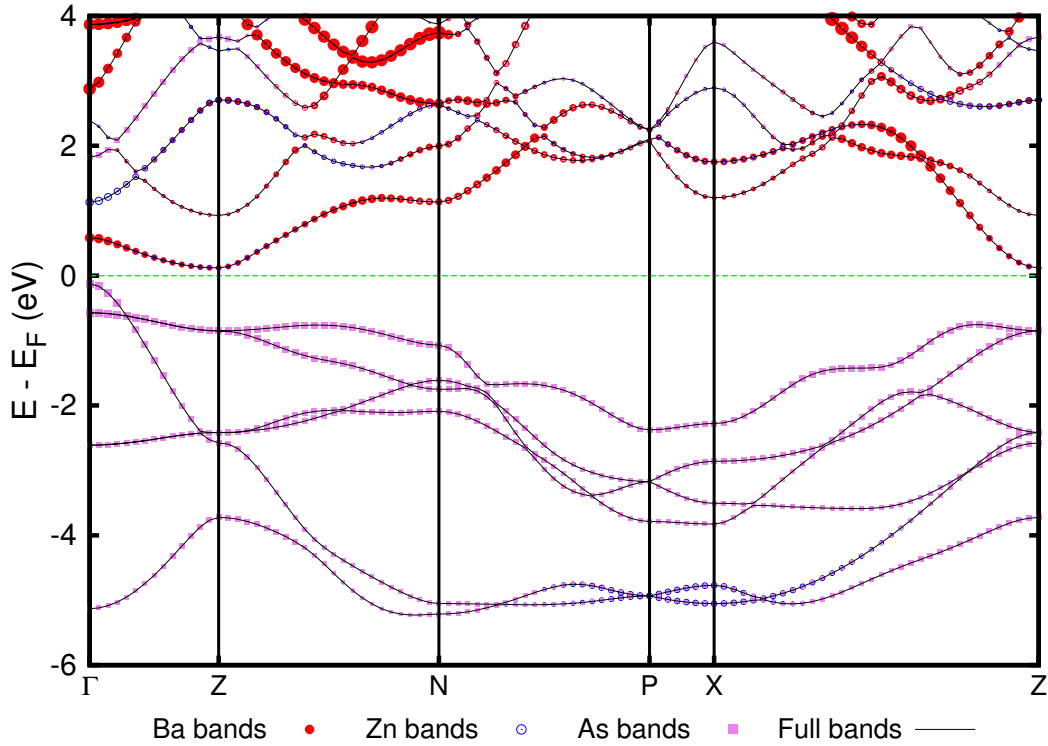


FIG. 4. (Color online) The character-resolved band structure of  $\text{BaZn}_2\text{As}_2$  calculated using the mBJ functional.

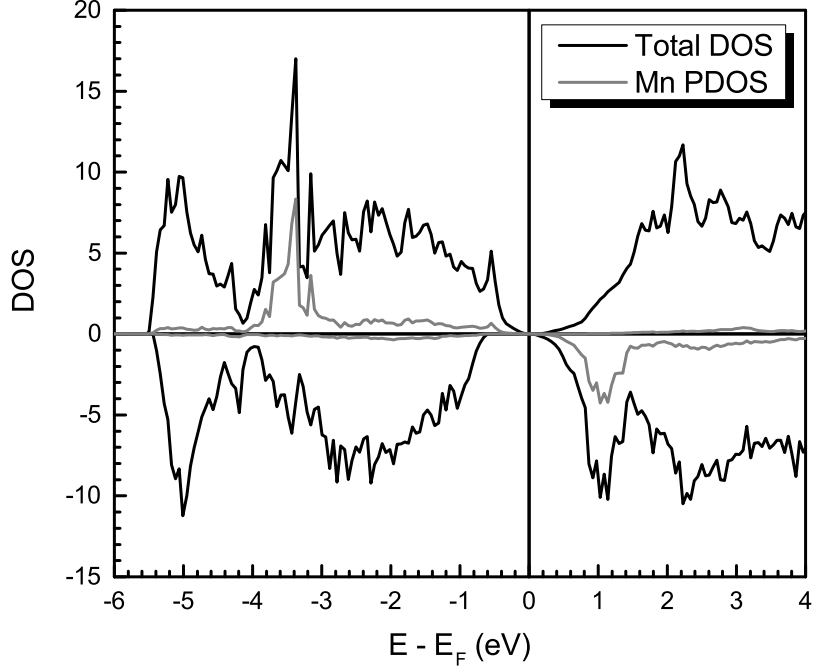


FIG. 5. The total density of states of  $\text{Ba}(\text{Zn}_{0.875}\text{Mn}_{0.125})_2\text{As}_2$  and the partial density of states for Mn calculated using the mBJ functional.

TABLE I. The supercells dimensions and intraplanar and interplanar Mn-Mn configurations used for fitting to Eq. (2). Each neighbor number entry represents two calculations, one for ferromagnetic alignment and another for antiferromagnetic alignment of the Mn atoms. The doping level  $y$  for two Mn atoms placed in the supercells is also reported.

Dimensions	$y$	Intraplane Neighbors	Interplane Neighbors
$2 \times 2 \times 1$	0.06250	1, 2, 3, 4, 5	1, 2, 3, 4, 6
$3 \times 3 \times 1$	0.02778	1, 2, 3, 4, 5, 6, 7	
$4 \times 2 \times 1$	0.03125	1, 2, 3, 6, 7	
$2 \times 2 \times 2$	0.03125		1, 2, 3, 4, 5

where  $\Delta E$  is the energy gained by forming a dimer compared with two isolated Mn atoms. We now minimize the free energy with respect to the number of dimers: we expand the logarithm again in  $1/n$ , take the derivative with respect to  $\kappa$ , and get

$$\begin{aligned} \ln \left[ \left( 2e^{\Delta E/T} (-2\kappa + y)^2 \right) / \kappa \right] \\ = \ln \left[ \left( 2\beta^{-1} (-2\kappa + y)^2 \right) / \kappa \right] = 0, \end{aligned} \quad (8)$$

where  $\beta = e^{-\Delta E/T}$ . Solving for  $\kappa$ , we get  $\kappa = (\beta + 8y - \sqrt{\beta^2 + 16\beta y})/16$ .

In the main text we established that nearest-neighbor dimers are AFM, and therefore each dimer results in the cancellation of two Mn moments from the total magnetization. Therefore the reduction coefficient (observed magnetization vs. maximum possible) can be defined as

$$r = 1 - 2\beta/y = (\sqrt{\beta^2 + 16\beta y} - \beta)/8y. \quad (9)$$

There are a couple of limiting cases that we should note. The first is the case of infinite energy gain, when  $\beta = 0$ . As expected,  $r = 0$  as all Mn atoms are paired into dimers. The second limiting case is that of no energy gain, when  $\beta = 1$ . In this case we should expect the solution to coincide with the “stochastic” solution,  $r = (1 - y)^4 + 4y^3(1 - y)$ , which is the computed probability that a given Mn atom forms, stochastically, a dimer with one or a tetramer with three neighboring Mn atoms (both combinations will cancel the involved Mn atoms’ contribution to the total magnetization). Our solution in Eq. (9), derived in the limit  $y \ll 1$ , is correct to the lowest order in  $y$ , yielding  $r = 1 - 4y + O(y^2)$ . In the next order our formula underestimates the reduction,  $r = 1 - 4y + 32y^2 + O(y^3)$  vs.  $r = 1 - 4y + 4y^2 + O(y^3)$ , and for  $y = 0.05$  the error is less than 5%.

*Stability of interstitial Mn impurities*—A common issue with the III-V dilute magnetic semiconductor compounds is that Mn doping can lead to both interstitial and substitutional impurities. Here we show that there is a large

TABLE II. The distances between Mn-Mn pair configurations and the magnitude and standard error of the exchange constants for both intraplanar ( $J_x^{\parallel}$ ) and interplanar ( $J_x^{\perp}$ ) couplings. The pairs are reported by their neighbor number as shown in the diagram in Fig. 3(b)

#	$r_{\parallel}$ (Å)	$J_x^{\parallel}(r_{\parallel})$ (meV)			$r_{\perp}$ (Å)	$J_x^{\perp}(r_{\perp})$ (meV)		
		$x = 0.0$	$x = 0.2$	$x = 0.4$		$x = 0.0$	$x = 0.2$	$x = 0.4$
1	2.921	200.7 ± 2.2	108.8 ± 10.3	60.6 ± 9.1	6.741	20.9 ± 2.0	-6.6 ± 2.7	-20.2 ± 2.9
2	4.131	81.4 ± 2.7	-3.1 ± 12.7	-43.2 ± 12.7	7.346	4.2 ± 1.9	-11.8 ± 2.7	-16.7 ± 2.9
3	5.842	-3.2 ± 1.1	-17.6 ± 5.1	-13.7 ± 4.5	7.906	3.2 ± 0.8	-7.2 ± 2.7	-9.746 ± 2.9
4	6.532	3.1 ± 1.1	-20.8 ± 5.4	-25.3 ± 4.7	8.920	0.9 ± 0.6	-2.3 ± 1.1	-3.0 ± 1.2
5	8.262	5.3 ± 0.5	-8.3 ± 2.4	-15.7 ± 2.1	9.386	1.2 ± 1.0	-1.3 ± 2.8	-4.1 ± 3.0
6	8.763	0.4 ± 1.0	-2.6 ± 4.8	-6.2 ± 4.2	10.663	0.3 ± 0.4	-0.5 ± 0.6	-1.8 ± 0.6
7	9.237	0.6 ± 0.8	-3.8 ± 4.0	-2.9 ± 3.5				

TABLE III. The calculated energies of the  $3 \times 3 \times 1$  supercell for intraplane Mn-Mn pair configurations with ferromagnetic (FM) and antiferromagnetic (AFM) alignment. The pairs are reported by their neighbor number as shown in the diagram in Fig. 3(b). The three pairs of columns are the three different hole-doping levels used for  $x$ .

#	$x = 0.0$ (eV)		$x = 0.2$ (eV)		$x = 0.4$ (eV)	
	FM	AFM	FM	AFM	FM	AFM
1	-626.8359	-627.2429	-428.9581	-429.1655	-322.1117	-322.2600
2	-626.9715	-627.1397	-429.0902	-429.0730	-322.2467	-322.1584
3	-627.0589	-627.0548	-429.1219	-429.0755	-322.2930	-322.2575
4	-627.0479	-627.0605	-429.1160	-429.0636	-322.2854	-322.2248
5	-627.0427	-627.0706	-429.1178	-429.0587	-322.2859	-322.2181
6	-627.0567	-627.0613	-429.1129	-429.1018	-322.2844	-322.2843
7	-627.0571	-627.0634	-429.1134	-429.0890	-322.2911	-322.2754

energy penalty for interstitial impurities in  $\text{BaZn}_2\text{As}_2$  using the methodology developed by Jenkins [39].

Let  $\mu_{\text{BaZn}_2\text{As}_2}^{\text{bulk}}$  be the bulk chemical potential of  $\text{BaZn}_2\text{As}_2$ ,  $\mu_{\text{BaAs}_2}^{\text{bulk}}$  the bulk chemical potential of a hypothetical structure of  $\text{BaAs}_2$ , and  $\mu_{\text{Zn}}^{\text{bulk}}$  the bulk chemical potential of Zn. The potentials of the constituents of  $\text{BaZn}_2\text{As}_2$  are subject to the constraint

$$\mu_{\text{BaZn}_2\text{As}_2}^{\text{bulk}} = 2\mu_{\text{Zn}} + \mu_{\text{BaAs}_2}. \quad (10)$$

The constituents of  $\text{BaZn}_2\text{As}_2$  are also related to their respective bulk chemical potentials in the following inequalities

$$\mu_{\text{BaAs}_2}^{\text{bulk}} > \mu_{\text{BaAs}_2}, \quad (11)$$

$$\mu_{\text{Zn}}^{\text{bulk}} > \mu_{\text{Zn}}. \quad (12)$$

It follows from combining Eqs. (10), (11), and (12) that  $\mu_{\text{Zn}}$  is subject to the following constraint,

$$\frac{\mu_{\text{BaZn}_2\text{As}_2}^{\text{bulk}} - \mu_{\text{BaAs}_2}^{\text{bulk}}}{2} < \mu_{\text{Zn}} < \mu_{\text{Zn}}^{\text{bulk}}. \quad (13)$$

In practice the bulk potentials are equivalent to the DFT energy, so to find them we calculate the total energy of bulk  $\text{BaZn}_2\text{As}_2$ , bulk Zn, and bulk  $\text{BaAs}_2$  [40].

Next we write down the Gibbs free energy for two Mn impurity scenarios. Let  $G_{\text{sub}}$  be the Gibbs free energy and  $E_{\text{sub}}$  be the calculated energy of the supercell with a substitutional impurity, and let  $G_{\text{int}}$  be the Gibbs free energy and  $E_{\text{int}}$  be the calculated energy of the supercell with an interstitial impurity. For our calculations, the chemical formula for the substitutional impurity supercell is  $\text{Ba}_8\text{Zn}_{15}\text{MnAs}_{16}$  and for the interstitial impurity it is  $\text{Ba}_8\text{Zn}_{16}\text{MnAs}_{16}$ , see Fig. 6 for a schematic representation. The following then is the Gibbs free energy of the supercells with either a substitutional or interstitial impurity:

$$G_{\text{sub}} = E_{\text{sub}} - 15\mu_{\text{Zn}} - 8\mu_{\text{BaAs}_2} - \mu_{\text{Mn}} \quad (14)$$

$$G_{\text{int}} = E_{\text{int}} - 16\mu_{\text{Zn}} - 8\mu_{\text{BaAs}_2} - \mu_{\text{Mn}} \quad (15)$$

It follows then that the difference in Gibbs free energy between the substitutional and interstitial configurations is given by

$$G_{\text{sub}} - G_{\text{int}} = E_{\text{sub}} - E_{\text{int}} + \mu_{\text{Zn}} \quad (16)$$

Using VASP, we calculate  $\mu_{\text{BaZn}_2\text{As}_2}^{\text{bulk}} = -16.98$  eV/f.u.,  $\mu_{\text{BaAs}_2}^{\text{bulk}} = -13.60$  eV/f.u.,  $\mu_{\text{Zn}}^{\text{bulk}} = -1.26$  eV/Zn,  $E_{\text{sub}} = -143.64$  eV, and  $E_{\text{int}} = -142.55$  eV. We find that the

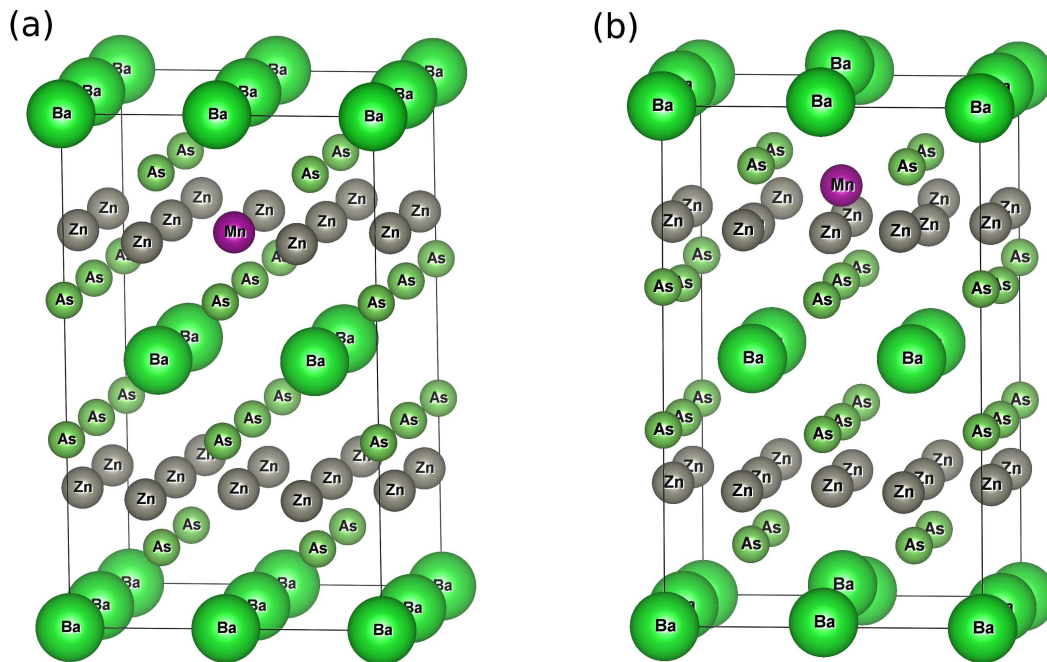


FIG. 6. The supercell configurations of  $\text{BaZn}_2\text{As}_2$  used to calculate the relative energetic stability of a substitutional vs. interstitial Mn impurity. (a) The relaxed structure of  $\text{Ba}_8\text{Zn}_{15}\text{MnAs}_{16}$  where Mn was substituted for a Zn atom. (b) The relaxed structure of  $\text{Ba}_8\text{Zn}_{16}\text{MnAs}_{16}$  where the Mn interstitial is in the empty space between neighboring As-Zn planes.

bounding for Zn is  $-1.69 \text{ eV} < \mu_{\text{Zn}} < -1.26 \text{ eV}$  and that  $G_{\text{sub}} - G_{\text{int}} = -1.09 \text{ eV} + \mu_{\text{Zn}}$ . Based on this analysis,

there is a substantial energetic preference of  $-2.6 \pm 0.2 \text{ eV}$  for the substitutional impurity.

- 
- [1] J. K. Furdyna, *J. Appl. Phys.* **64**, R29 (1988).  
 [2] H. Ohno, *Science* **281**, 951 (1998).  
 [3] T. Dietl, *Nat. Mater.* **9**, 965 (2010).  
 [4] T. Jungwirth, J. Sinova, J. Mašek, J. Kucera, and A. H. MacDonald, *Rev. Mod. Phys.* **78**, 809 (2006).  
 [5] I. Žutić, J. Fabian, and S. D. Sarma, *Rev. Mod. Phys.* **76**, 323 (2004).  
 [6] S. Koshihara, A. Oiwa, M. Hirasawa, S. Katsumoto, Y. Iye, C. Urano, H. Takagi, and H. Munekata, *Phys. Rev. Lett.* **78**, 4617 (1997).  
 [7] H. Ohno, D. Chiba, F. Matsukura, T. O. E. Abe, T. Dietl, Y. Ohno, and K. Ohtani, *Nature* **408**, 944 (2000).  
 [8] A. G. Petukhov, I. Žutić, and S. C. Erwin, *Phys. Rev. Lett.* **99**, 257202 (2007).  
 [9] M. Tanaka, S. Ohya, and P. N. Hai, *Appl. Phys. Rev.* **1**, 011102 (2014).  
 [10] M. Dobrowolska, K. Tivakornsasithorn, X. Liu, J. Furdyna, M. Berciu, K. M. Yu, and W. Waluliewicz, *Nature Materials* **11**, 444 (2012).  
 [11] T. Dietl, H. Ohno, F. Matsukura, J. Cibert, and D. Ferrand, *Science* **287**, 1019 (2000).  
 [12] M. Sawicki, T. Devillers, S. Galeski, C. Simserides, S. Dobkowska, B. Faina, A. Grois, A. Navarro-Quezada, K. N. Trohidou, J. A. Majewski, T. Dietl, and A. Bonanni, *Phys. Rev. B* **85**, 205204 (2012).  
 [13] Z. Deng, C. Q. Jin, Q. Q. Liu, X. C. Wang, J. L. Zhu, S. M. Feng, L. C. Chen, R. C. Yu, C. Arguello, T. Goko, F. Ning, J. Zhang, Y. Wang, A. A. Aczel, T. Munsie, T. J. Williams, G. M. Luke, T. Kakeshita, S. Uchida, W. Higemoto, T. U. Ito, B. Gu, S. Maekawa, G. D. Morris, and Y. J. Uemura, *Nature Comm.* **2**, 422 (2011).  
 [14] Z. Deng, K. Zhao, B. Gu, W. Han, J. L. Zhu, X. C. Wang, X. Li, Q. Q. Liu, R. C. Yu, T. Goko, B. Frandsen, L. Liu, J. Zhang, Y. Wang, F. L. Ning, S. Maekawa, Y. J. Uemura, and C. Q. Jin, *Phys. Rev. B* **88**, 081203 (2013).  
 [15] K. Zhao, Z. Deng, X. C. Wang, W. Han, J. L. Zhu, X. Li, Q. Q. Liu, R. C. Yu, T. Goko, B. Frandsen, L. Liu, F. Ning, Y. J. Uemura, H. Dabkowska, G. M. Luke, H. Luetkens, E. Morenzoni, S. R. Dunsiger, A. Senyshyn, P. Böni, and C. Q. Jin, *Nature Comm.* **4**, 1442 (2013).  
 [16] K. Zhao, B. Chen, G. Q. Zhao, X. Li, Z. Yuan, Z. Deng, Q. Q. Liu, and C. Q. Jin, *Chinese Science Bulletin* (2014), in press.  
 [17] H. Man, C. Ding, S. Guo, G. Zhi, X. Gong, Q. W. and H. Wang, B. Chen, and F. L. Ning, arXiv:1403.4019 (2014), preprint.  
 [18] D. Khomskii, *Basic Aspects of the Quantum Theory of Solids* (Cambridge University Press, Cambridge, 2010).  
 [19] C. Zener, *Phys. Rev.* **82**, 403 (1951).  
 [20] M. A. Ruderman and C. Kittel, *Phys. Rev.* **96**, 99 (1954).

- [21] T. Kasuya, *Prog. Theor. Phys.* **16**, 45 (1956).
- [22] K. Yosida, *Phys. Rev.* **106**, 893 (1957).
- [23] E. L. Nagaev, *Physics of Magnetic Semiconductors* (Mir, Moscow, 1983).
- [24] G. Kresse and J. Hafner, *Phys. Rev. B* **47**, R558 (1993).
- [25] G. Kresse and J. Furthmüller, *Phys. Rev. B* **54**, 11169 (1996).
- [26] ELK FP-LAPW Code [<http://elk.sourceforge.net/>].
- [27] P. Blaha, K. Schwarz, G. K. H. Madsen, K. Kvasnicka, and J. Luitz, Computer code WIEN2K (Karlheinz Schwarz, Techn. Universitat Wien, Austria, 2001).
- [28] J. P. Perdew, K. Burke, and M. Ernzerhof, *Phys. Rev. Lett.* **77**, 3865 (1996).
- [29] A. D. Becke and E. R. Johnson, *J. Chem. Phys.* **124**, 221101 (2006).
- [30] F. Tran and P. Blaha, *Phys. Rev. Lett.* **102**, 226401 (2009).
- [31] I. R. Shein and A. L. Ivanovskii, *J. All. Com.* **583**, 100 (2014).
- [32] The difference is due to different space partitioning in different codes.
- [33] While the relevant hopping amplitudes  $t_{pd}$  differ from orbital to orbital, for our purpose introducing one effective parameter is sufficient.
- [34] J. Cibert and D. Scalbert, in *Spin Physics in Semiconductors*, Springer Series in Solid-State Sciences, Vol. 157, edited by M. I. Dyakonov (Springer, Berlin Heidelberg, 2008) Chap. 13, pp. 389–431.
- [35] Magnetic interactions in itinerant systems do not always follow the Heisenberg law, so the mapping is never exact, but it gives us a good visual picture.
- [36] The actual protocol involves a long annealing at  $T \approx 1000$  K and then a very slow cooling to 300 K [15].
- [37] Similar reasoning has been put forth before, see H. Akai, *Phys. Rev. Lett.* **81**, 3002 (1998).
- [38] J. K. Glasbrenner and I. I. Mazin, *Phys. Rev. B* **89**, 060403(R) (2014).
- [39] S. J. Jenkins, *Phys. Rev. B* **70**, 245401 (2004).
- [40] A. Jain, S. P. Ong, G. Hautier, W. Chen, W. D. Richards, S. Dacek, S. Cholia, D. Gunter, D. Skinner, G. Ceder, and K. A. Persson, *APL Mat.* **1**, 011002 (2013).